

This is a copy of the published version, or version of record, available on the publisher's website. This version does not track changes, errata, or withdrawals on the publisher's site.

Strong impact of low-level substitution of Mn by Fe on the magnetoelectric coupling in TbMn O₃






A. Maia, R. Vilarinho, P. Proschek, M. Lebeda, M. Mihalik, Jr., M. Mihalik, P. Manuel, D. D. Khalyavin, S. Kamba, and J. Agostinho
Moreira

Published version information

Citation: A. Maia (et. al.) Strong impact of low-level substitution of Mn by Fe on the magnetoelectric coupling in TbMn O₃, Phys. Rev. Materials 8, 084405

DOI: <https://doi.org/10.1103/PhysRevMaterials.8.084405>

This version is made available in accordance with publisher policies. Please cite only the published version using the reference above. This is the citation assigned by the publisher at the time of issuing the APV. Please check the publisher's website for any updates.

Strong impact of low-level substitution of Mn by Fe on the magnetoelectric coupling in TbMnO₃A. Maia ¹, R. Vilarinho ², P. Proschek,³ M. Lebeda,¹ M. Mihalik, Jr. ⁴, M. Mihalik,⁴ P. Manuel,⁵ D. D. Khalyavin,⁵ S. Kamba ¹ and J. Agostinho Moreira ²¹*Institute of Physics of the Czech Academy of Sciences, Na Slovance 2, 182 00 Prague, Czech Republic*²*IFIMUP, Physics and Astronomy Department, Faculty of Sciences, University of Porto, 4169-007 Porto, Portugal*³*Faculty of Mathematics and Physics, Charles University, Ke Karlovu 5, 121 16 Prague, Czech Republic*⁴*Institute of Experimental Physics Slovak Academy of Sciences, Watsonova 47, 040 01 Košice, Slovak Republic*⁵*ISIS Facility, Rutherford Appleton Laboratory, Harwell Campus, Didcot OX11 0QX, United Kingdom*

(Received 20 December 2023; revised 29 February 2024; accepted 24 July 2024; published 9 August 2024)

The correlation between static magnetoelectric coupling and magnetic structure was investigated in TbMn_{0.98}Fe_{0.02}O₃ with magnetic field up to 8 T and down to 2 K. Single-crystal neutron diffraction experiments reveal a substantial increase in the temperature dependence of the incommensurate modulation wave vector of the antiferromagnetic phase as the magnetic field strength increases. Magnetic field-dependent pyroelectric current measurements revealed significantly higher magnetoelectric coupling at magnetic fields below 4 T than in pure TbMnO₃. This is due to the higher sensitivity of the incommensurably modulated cycloid structure to weak magnetic fields. Detailed analysis of our data confirmed that the ferroelectric polarization is induced by inverse Dzyaloshinskii-Moriya interaction for magnetic field strength up to 4 T, but at higher fields a departure from theoretical predictions is ascertained, giving evidence for an additional, as yet misunderstood, contribution to magnetoelectric coupling. It shows that a small 2% substitution of Mn³⁺ by Fe³⁺ has a strong impact on the magnetic structure, promoting the destabilization of the incommensurably modulated magnetic cycloidal structure of TbMnO₃ in a magnetic field above 5 T. We demonstrate that the magnetoelectric coupling magnitude can be tuned through suitable substitutional elements, even at low level, inducing local lattice distortions with different electronic and magnetic properties.

DOI: [10.1103/PhysRevMaterials.8.084405](https://doi.org/10.1103/PhysRevMaterials.8.084405)

I. INTRODUCTION

Magnetoelectric multiferroics, where spontaneous long-range magnetic ordering and ferroelectricity coexist and are coupled, represent a very attractive class of compounds combining rich and fascinating fundamental physics [1,2]. A key point to be studied in this report is the effect of controlled chemical substitution on the relationship between structure, magnetism, ferroelectricity, and magnetoelectric coupling. In this regard, the solid solution TbMn_{1-x}Fe_xO₃ proved to be a suitable system to unravel such delicate coupling between magnetism and ferroelectricity [3–6]. Although the Mn³⁺ cation is Jahn-Teller active, unlike the Fe³⁺ cation, they have the same ionic radius for the sixth coordination, allowing one to synthesize isostructural solid solutions in the entire x range. However, the substitution of Mn³⁺ by Fe³⁺ implies a change in the octahedra distortions of perovskite lattice, with a high impact on the magnetic and polar properties. Previous experimental studies in TbMn_{1-x}Fe_xO₃ at ambient temperature have evidence for the linear decrease of the cooperative Jahn-Teller distortion amplitude for $0 \leq x \leq 0.5$, and its suppression for higher Fe concentrations [7]. Furthermore, the octahedra tilting has been found to be sensitive to the amplitude of the Jahn-Teller distortion, which gives clear evidence for the role played by the interplay between structure and magnetism, with impact on the ferroelectric stabilization [7].

TbMnO₃ is a type-II multiferroic [8] prototype with a large magnetoelectric coupling. Its phase diagram can be summarized as follows. At room conditions, TbMnO₃ is a paraelectric paramagnet with orthorhombic crystal structure described by the $Pbnm$ space group [8]. At $T_N = 41$ K, TbMnO₃ undergoes an antiferromagnetic (AFM) phase transition, with incommensurate sinusoidal collinear order of the Mn³⁺ spins [9,10]. In this phase, the spins are aligned along the b axis with a temperature-dependent propagation vector, taking the value $\mathbf{q}_m = (00.291)$ at T_N [9,10]. Accompanying the magnetic modulation structure, there is a lattice modulation with the wave vector found to be $\mathbf{k}_1 = 2\mathbf{q}_m$ [11,12]. Below $T_C = 28$ K, the sinusoidal spin modulation turns into a cycloidal spiral in the bc plane, as revealed by neutron diffraction studies [9,10]. Whether the magnetic modulation remains incommensurate or changes into commensurate is still a matter of debate, since it becomes weakly temperature-dependent below T_C but not completely locking in a fixed commensurate value [9–11,13]. The emergence of a spontaneous electric polarization along the c axis coincides with the cycloid spin ordering below T_C , implying an intrinsic entanglement between the spiral-type antiferromagnetism and ferroelectricity [8,14]. According to Aliouane *et al.* [15], TbMnO₃ exhibits quadratic magnetoelastic coupling in the absence of applied magnetic field. Still, a linear magnetoelastic coupling emerges in TbMnO₃ when an external magnetic field is applied along the b axis, so that ferroelectricity is no longer a secondary effect [15]. The linear magnetoelastic cou-

pling drives a magneto-structural transition from the cycloidal modulated phase, with the spontaneous polarization along the c axis, to a phase with the spontaneous polarization along the a axis, for a magnetic field higher than 4.5 T [14]. When the external field is applied along the a axis, a similar flop is found but at higher critical field of about 9 T [14]. Upon further temperature decrease, a quasi-long-range ordering of the f electrons spins of the Tb^{3+} ions takes place below $T_N^{\text{Tb}} \approx 7$ K [9,10].

In general, the isovalent partial substitution of Mn by Fe ($\text{TbMn}_{1-x}\text{Fe}_x\text{O}_3$) modifies the sequence of phase transitions [5]. However, for low-level substitution, corresponding to $0 < x < 0.05$, the phase sequence is found to be the same as in TbMnO_3 , although both T_N and T_C decrease with increasing x , while T_N^{Tb} barely shifts [6]. The critical temperatures decrease with increasing x gives clear evidence for the destabilization of the magnetic interactions underlying the magnetic properties [6]. The main outcome concerns the decrease of the maximum electric polarization as Fe^{3+} content increases towards $x = 0.04$, which has been attributed to the gradual fading out of the cycloidal spin ordering with increasing x , and the suppression of ferroelectricity for $x \geq 0.05$ [6].

Most of the previous studies in the multiferroic region of the $\text{TbMn}_{1-x}\text{Fe}_x\text{O}_3$ solid solution ($0 < x < 0.05$) relied on polycrystalline samples, losing information regarding the anisotropic properties of both polarization and magnetism [4,6]. Because such features play important roles in the pure compound, they are assumed to be particularly important in the multiferroic region of the solid solution as well. In particular, the direction of the applied magnetic field should have interesting effects on the magnetic structure, some of which is inferred by the direction of polarization switching from the c to the a axis [14]. To understand in more detail the magnetic structure and magnetoelectric coupling of low-level Fe-substituted TbMnO_3 , we performed a detailed study of the temperature and magnetic field dependence of the ferroelectric polarization of oriented $\text{TbMn}_{0.98}\text{Fe}_{0.02}\text{O}_3$ single crystals. Neutron diffraction data in $\text{TbMn}_{0.98}\text{Fe}_{0.02}\text{O}_3$ are discussed in connection with the results of polarization measurements, towards the characterization of the magnetoelectric coupling. The systematic study of magnetoelectric phenomena provides a deeper understanding of the effect of the B-site cation on the microscopic mechanisms underlying the magnetic and polar properties in TbMnO_3 .

II. EXPERIMENTAL DETAILS

High-quality $\text{TbMn}_{0.98}\text{Fe}_{0.02}\text{O}_3$ single crystals were grown by the floating zone method in an FZ-T-4000 (Crystal Systems Corporation) mirror furnace, using MnO_2 , Tb_4O_7 , and Fe_2O_3 as starting materials. The starting powders were mixed in the intended Tb:Mn:Fe stoichiometric ratio, cold pressed into rods, and sintered at 1100 °C for 12–14 h in air. Growing was performed in air atmosphere, feed and seed rod were rotated with a speed of 30 rpm in opposite directions, and a pulling speed of 6 mm/h was used. The typical length of a grown ingot was between 3 and 5 cm [3,4]. The obtained ingot was oriented using Laue diffraction patterns, and special care was taken to avoid macle. The samples were cut from a macle-free region of the oriented ingot. The samples were

first characterized by x-ray diffraction and Raman scattering at room temperature, and temperature-dependent magnetization and specific heat. The obtained results are in good agreement with published data [3,4].

The pyroelectric currents were measured in a standard Quantum Design PPMS while heating at a rate of 5 K min^{-1} , after cooling under a fixed applied magnetic field. The pyroelectric current measurements were performed after poling the crystals with an electric field of 100 V mm^{-1} , while cooling from a temperature above the Néel temperature. Before measuring, the poling electric field was turned off at 2 K. The temperature dependence of the electric polarization was obtained through time integration of the measured pyroelectric currents.

Single-crystal neutron diffraction under applied magnetic field was measured at Wish beamline of the ISIS Neutron and Muon Source at the Rutherford Appleton Laboratory of the Science and Technology Facilities Council. Single-crystal neutron diffraction patterns were recorded at fixed temperatures between 5 and 50 K after cooling the sample under an applied magnetic field along the b axis, up to 8 T. The sample was inserted in a helium flow Oxford cryostat, placed in such a way that the b axis is oriented in the vertical direction, parallel to the applied magnetic field, generated by a 9 T magnet. This magnet has an 80° window in the horizontal and a 30° one in the vertical directions. Due to the magnet surrounding the sample, only a restricted angle range could be measured. With this configuration, a limited number of nuclear and magnetic diffraction peaks could be studied as a function of temperature and magnetic field, with the condition that the (hkl) peaks have $k = 0$ or $k = q_{\text{Mn}}$.

III. RESULTS

A. Polar properties under magnetic field

This section is focused on the temperature dependence of the electric polarization, obtained in the following measurement configurations: $\mathbf{E}||a$ and $\mathbf{B}||b$, and $\mathbf{E}||c$ and $\mathbf{B}||a, b$, and c , for which the largest effects of the applied magnetic field on the polar properties of $\text{TbMn}_{0.98}\text{Fe}_{0.02}\text{O}_3$ are found.

Figures 1(a) and 1(b) show the temperature dependence of the pyroelectric current density, $J(T)$, of $\text{TbMn}_{0.98}\text{Fe}_{0.02}\text{O}_3$ measured along the a and c axes, respectively, under an applied magnetic field (0–9 T) along the b axis. The corresponding temperature dependence of the electric polarization, along the a and c axis, obtained from the time integration of the pyroelectric current density, is presented in Figs. 1(c) and 1(d), respectively. At 0 T, the pyroelectric current density measured along the c axis, $J_c(T)$, peaks at $T_C = 23$ K, as expected according to earlier reports for $\text{TbMn}_{0.98}\text{Fe}_{0.02}\text{O}_3$ ceramics, evidencing the onset of the ferroelectric phase, with spontaneous electric polarization along the c axis [6]. This anomaly slightly downshifts with increasing magnetic field strength, reaching 21 K at 9 T.

A second anomaly in $J_c(T)$ is observed at lower temperatures, but only for a magnetic field strength above 2 T. This anomaly peaks in opposite sense relatively to the first one, and monotonously upshifts from 6 K, for 2 T, to 14 K, for 9 T. Its amplitude exhibits a nonmonotonous magnetic field dependence, being maximum at 5 T. At 0 T, $P_c(T)$

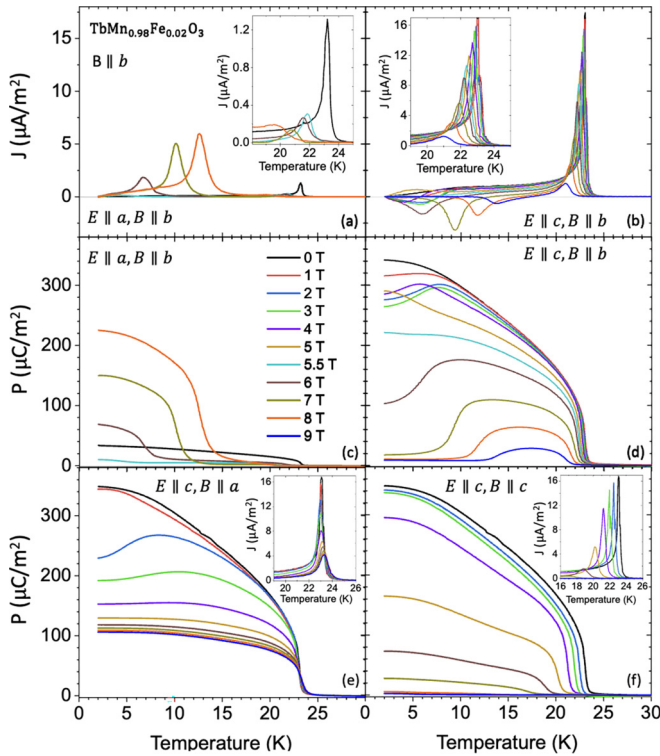


FIG. 1. Temperature dependence of the (a), (b) pyroelectric current densities and (c), (d) electric polarization of $\text{TbMn}_{0.98}\text{Fe}_{0.02}\text{O}_3$, measured along the a and c axes under an applied magnetic field along the b axis. The insets show a magnified view of the temperature profiles of the pyroelectric current density.

monotonously increases on cooling from $T_C = 23$ K, and its value at 2 K is $350 \mu\text{C}/\text{m}^2$, 58% smaller than the maximum polarization observed in TbMnO_3 after poling in twice higher field (200 V mm^{-1}) [14]. The decrease of the P_c value in $\text{TbMn}_{0.98}\text{Fe}_{0.02}\text{O}_3$ has been reported as a consequence of the destabilization of the magnetic structure due to the changes in magnetic interactions promoted by Fe^{3+} [6]. As the magnetic field increases toward 3 T, $P_c(T)$ shows a maximum, peaking at highest temperatures according to the magnetic field strength, and then shifts to lower temperatures on further magnetic field increase up to 5 T. Interestingly, the value of P_c at fixed temperatures decreases at a faster magnetic field rate for $B > 5.5$ T. The $P_c(T)$ curve changes its shape for at 6 T, fading out with decreasing temperature, in such a way that for 9 T, $P_c \sim 0$ below 13 K. Contrarily to TbMnO_3 , the magnetic field evolution of $P_c(T)$, with $B \parallel b$ is more gradual in this compound [14].

Concerning the temperature dependence of the pyroelectric current density recorded along the a axis, $J_a(T)$, a small anomaly at $T_C = 23$ K is already observed for 0 T contrary to pure TbMnO_3 , where no anomaly was detected [14]. As the magnetic field strength increases, the amplitude of this anomaly decreases and downshifts, following a similar temperature trend as observed for $J_c(T)$ [see inset of Fig. 1(a)]. Due to the similar temperature behavior, we assign this anomaly to the minor electric polarization projection in the measurement direction, due to a small misorientation in the sample. A second anomaly in $J_a(T)$ emerges at low tempera-

tures with the same sign as the first one. The second anomaly peaks at higher temperatures, and its amplitude increases as the magnetic field strength increases. These results evidence the enhancement of the electric polarization along the a axis as the magnetic field increases, as seen in Fig. 1(c). The maximum electric polarization along the a axis, recorded at 2 K and 8 T, is about 70% of the maximum spontaneous polarization value measured at the same temperature along the c axis, in the absence of the applied magnetic field. In TbMnO_3 , the maximum value of the electric polarization along the a axis is about 67% of the maximum value of the electric polarization from the c axis, after the magnetically induced polarization flop [14].

Figure 1(e) shows the temperature dependence of the electric polarization measured under applied magnetic field along the a axis ($B \parallel a$). The pyroelectric current $J_c(T)$, shown in the inset of Fig. 1(e), exhibits just one anomaly, peaking at $T_C = 23$ K, weakly dependent on the field strength. However, the amplitude of this anomaly decreases with increasing field strength; consequently, the electric polarization is a decreasing function of the magnetic field strength, gradually converging to the limit value $110 \mu\text{C}/\text{m}^2$, contrarily to what is observed when the magnetic field is applied along the other two crystallographic axes. At 9 T, the value of P_c at the lowest temperature is 25% of the value obtained in TbMnO_3 which, however, was poled at twice higher electric field [14].

Figure 1(f) depicts the temperature dependence of the electric polarization and pyroelectric current [inset of Fig. 1(f)] measured along the c axis, under different magnetic field strength, applied along the same c axis. Only one anomaly is observed in $J_c(T)$ for all the values of the field strength; as consequence, at a fixed magnetic field, the electric polarization increases monotonously on cooling below T_C . Moreover, the $J_c(T)$ anomaly peaks at $T_C = 23$ K for 0 T, monotonously decreasing the peaking temperature as the magnetic field increases, reaching 16 K for 9 T [see inset of Fig. 1(f)]. The amplitude of this anomaly also decreases and eventually disappears for $B > 9$ T, meaning that the electric polarization is a decreasing function of the applied magnetic field along the c axis, reaching negligible values for 9 T. The latter result contrasts with the temperature/magnetic field dependence of the electric polarization of TbMnO_3 measured in the same configuration but poled at twice higher electric field [14]. In fact, for $B < 6$ T, $P_c(T)$ is weakly dependent on the magnetic field, increasing with decreasing temperature, although a change of slope of $P_c(T)$ is observed just below 10 K [14]. However, as the magnetic field increases further from 6 T, the $P_c(T)$ curve profile changes, and, for 8 and 9 T, the electric polarization takes non-negligible values between T_C and 15 K [14].

B. Neutron diffraction

In this section, we will address the temperature and magnetic field dependencies of the measured nuclear and magnetic diffraction peaks. Figure 2 shows representative neutron diffraction patterns, recorded at fixed temperatures in the 5–50 K range, and fixed magnetic field strength (0–8 T range), applied along the b axis. The results recorded for other magnetic field strengths and same temperatures, are

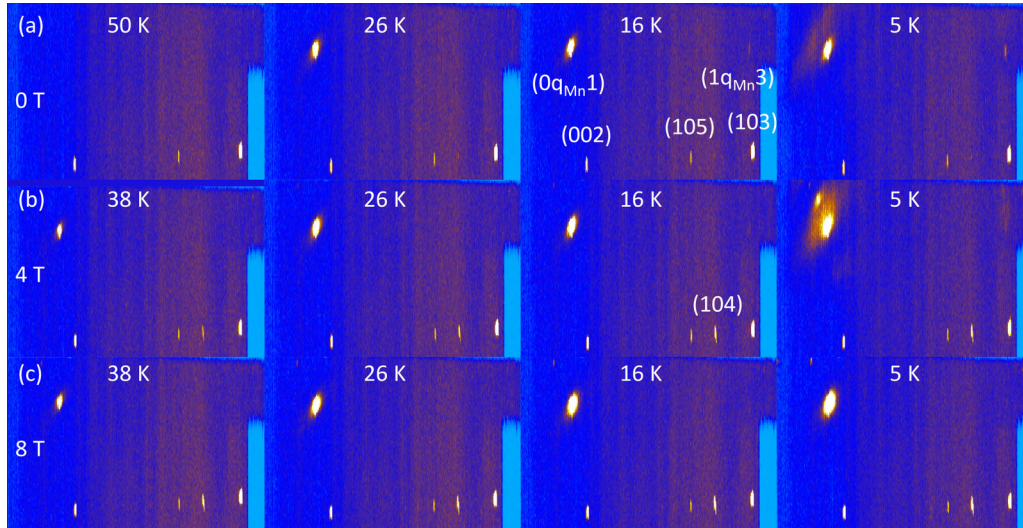


FIG. 2. Diffraction patterns of $\text{TbMn}_{0.98}\text{Fe}_{0.02}\text{O}_3$, recorded at different fixed temperatures and magnetic fields of 0 T (a), 4 T (b), and 8 T (c), applied along the b axis.

shown in Fig. S1 of the Supplemental Material [16]. Only the upper half part of the detectors panel is presented, with the main observed diffraction peaks indexed. Experimental restrictions, due to the configuration of the magnets, prevented us from collecting enough diffraction peaks to determine the real space spin structure.

Above $T_N = 39$ K, only nuclear peaks are observed and are indexed to reflections from the (0 0 2), (1 0 5), and (1 0 3) crystallographic planes. From the analysis of these peaks, the temperature and magnetic field dependence of the a and c lattice parameters was determined, as shown in Fig. S2 of the Supplemental Material for 0 and 8 T, respectively [16]. The lattice parameters slightly decrease with decreasing temperature in the 5–50 K range, and their values are magnetic field independent. These results evidence the negligible influence of both the magnetic phase transitions and the applied magnetic field on the lattice parameters, within the sensitivity of the diffraction technique. However, this does not mean that the magnetic phase transitions do not involve atomic motions, because the inversion center must be broken for the electric polarization to appear. Recently, spin-phonon coupling was ascertained from a temperature-dependent Raman scattering study in $\text{TbMn}_{0.98}\text{Fe}_{0.02}\text{O}_3$, where small anomalies in the temperature dependence of the wavenumber of some phonons assigned to Tb oscillations and symmetrical stretching mode of the oxygen octahedra were detected [3]. However, the magnetoelastic coupling is rather small in this compound to be observed through neutron diffraction techniques.

As the temperature decreases from $T_N = 39$ K, well-defined magnetic diffraction peaks appear along with the nuclear diffraction peaks (see Fig. 2). This is the case of the magnetic superlattice peak attributed to the Mn^{3+} moment ordering with propagation wave vector $(0 q_{\text{Mn}} 1)$ (q_{Mn} is expressed in reciprocal lattice units, r.l.u.), which appears just below T_N , as was also reported for TbMnO_3 [9,10,12]. This peak is observed in the 0–8 T magnetic field strength range. On further cooling, a second magnetic superlattice peak appears, but only below $T_C = 23$ K. Following Kajimoto *et al.*, we assign this peak to the G -type propagation wave vec-

tor $(1 q_{\text{Mn}} 3)$ of the Mn^{3+} moment ordering structure; the intensity of the $(1 q_{\text{Mn}} 3)$ magnetic superlattice peak strongly increases below T_C of TbMnO_3 , being negligibly small above this temperature [10]. Due to the limited q space covered in this experiment, we could not observe the Tb^{3+} magnetic superlattice peaks. Still, the Tb^{3+} spin ordering is ascertained from the appearance of other magnetic superlattice peaks and a strong diffuse scattering around the $(0 q_{\text{Mn}} 1)$ peak. Under applied magnetic field, we observe an additional Bragg peak indexed to $(1 0 4)$ and assigned to a (weak) ferromagnetic spin ordering, likely associated with a spin canting induced by the applied field. In the following, we shall address the temperature and magnetic field dependencies of the magnetic diffraction peaks.

Figure 3(a) shows the temperature dependence of the intensity of the magnetic superlattice peak $(0 q_{\text{Mn}} 1)$, recorded at 0, 4, 6, and 8 T, as representative examples. On cooling below $T_N = 39$ K, the intensity of this reflection increases and is enhanced by the applied magnetic field, the effect being more pronounced in the temperature range of the ferroelectric phase. A detailed analysis of the temperature dependence of the intensity of the magnetic superlattice peak $(0 q_{\text{Mn}} 1)$ reveals a small magnetic field-dependent kink at T_C , which, for the case of $B = 0$ T as a representative example, can be clearly observed in the inset of Fig. 3(a), where the solid line describes the temperature-dependent intensity, $I(T)$, in the $T_C < T < T_N$ range, extrapolated for $T < T_C$. The small but clear deviation of the experimental intensity on cooling below T_C was also reported for TbMnO_3 [9,10], and it gives clear evidence for the interplay between magnetism and ferroelectricity in these compounds. On further cooling, the intensity of the reflection exhibits different temperature behavior, depending on the magnetic field strength: while for 0 T and 4 T, a maximum is ascertained at 10 K, a sudden increase of the intensity at 10 K and at 14 K is observed for 6 T and 8 T, respectively. The temperature dependence of the modulation wave number q_{Mn} , determined from the magnetic superlattice peak $(0 q_{\text{Mn}} 1)$ position, recorded for different field strengths,

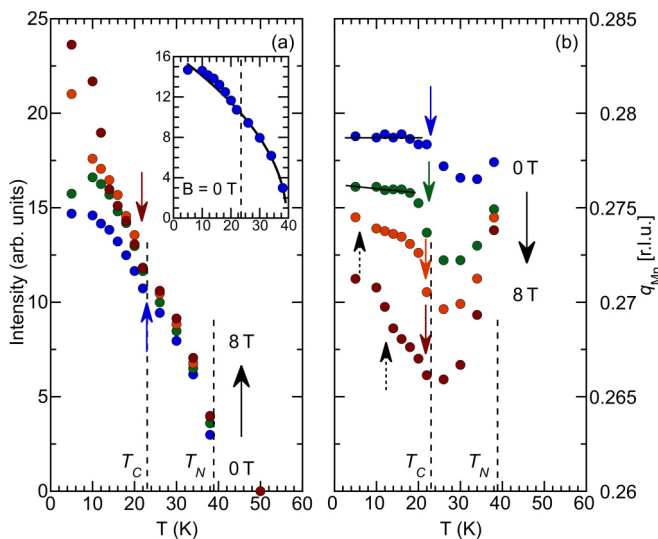


FIG. 3. Temperature dependencies of the (a) intensity and (b) q_{Mn} of the magnetic superlattice peak ($0 q_{Mn} 1$), recorded at 0, 4, 6, and 8 T, as representative examples. The vertical dashed lines mark the Mn^{3+} magnetic ordering temperatures at 0 T. The colored arrows point at the critical temperature T_C where the pyroelectric current density curve exhibits maximum value, while the black dashed arrows in (b) point at the temperatures where anomalous increasing of q_{Mn} is ascertained. Inset: Temperature dependence of the magnetic superlattice peak measured at $B = 0$ T. The solid line represents the temperature trend of the peak intensity in the $T_C < T < T_N$ range, extrapolated to $T < T_C$.

is presented in Fig. 3(b). In the absence of an applied magnetic field and at 38 K, $q_{Mn} = 0.278$, which is about 18% smaller than $q_{Mn} = 0.295$ reported for $TbMnO_3$ just below T_N , which evidences for a longer magnetic modulation wavelength in $TbMn_{0.98}Fe_{0.02}O_3$ [9,10,17]. In the whole temperature range here explored, q_{Mn} is a nonmonotonous function of temperature, although the temperature dependence is a function of the magnetic field. In the $T_C < T < T_N$ interval, q_{Mn} reaches a minimum value at temperatures approaching T_C as the magnetic field increases (32 K for 0 T and 24 K for 8 T). The relative variation of q_{Mn} in the $T_C < T < T_N$ range is 0.7%, a much smaller value when compared with $TbMnO_3$, for which the total variation in the sinusoidal incommensurate phase is 3.7% [17].

In the absence of the applied magnetic field, $q_{Mn}(T)$ of $TbMnO_3$ decreases on cooling and remains almost temperature independent below T_C , reaching values 0.276 in Refs. [9,10] and 0.28 in Ref. [17]. In $TbMn_{0.98}Fe_{0.02}O_3$, $q_{Mn}(T)$ slightly increases below 35 K and finally saturates near 0.279. Therefore, the temperature dependence is different between T_N and T_C , although the modulation wave vector in the ferroelectric phase takes similar value, within measurement accuracy, in the pure and iron-substituted samples.

The most significant changes induced by the magnetic field concerning the temperature dependence of q_{Mn} are observed below T_C . For $B \leq 5$ T, $q_{Mn}(T)$ is a slowly varying temperature function on cooling in such a way that an almost constant plateau is reached, while for $B \geq 6$ T, q_{Mn} is strongly temperature dependent, increasing as temperature decreases. At

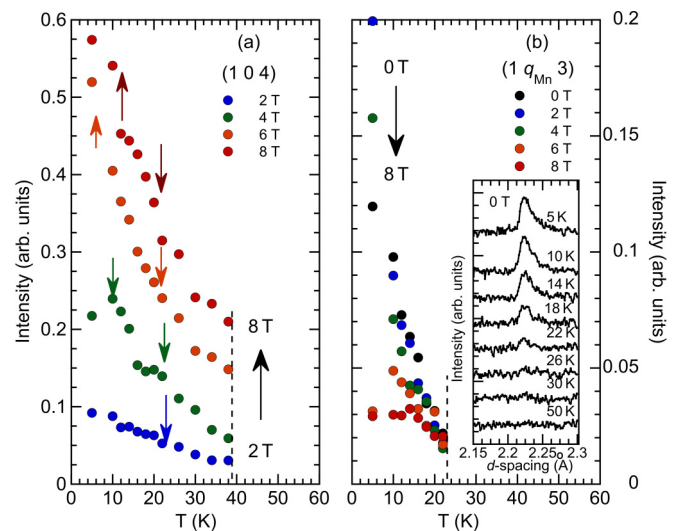


FIG. 4. Temperature dependence of (a) the intensity of the (1 0 4) magnetic diffraction peak and (b) the intensity of the magnetic superlattice peak ($1 q_{Mn} 3$) for $TbMn_{0.98}Fe_{0.02}O_3$, recorded at different fixed magnetic field strength. The colored arrows point at the critical temperature where the pyroelectric current density curve exhibits maximum value. Inset: Neutron diffraction pattern recorded at different fixed temperatures and in the absence of applied field, showing the magnetic superlattice peak ($1 q_{Mn} 3$).

8 T, the relative variation of q_{Mn} between T_C and the base temperature is 0.9%. The magnetic field threshold ($B \sim 5.5$ T) is the one for which the polarization flop is observed [see Figs. 1(c) and 1(d)]. The increasing of $q_{Mn}(T)$ on cooling from T_C contrasts with the observations in $TbMnO_3$, for which at 5.5 T a decrease on cooling is observed [12].

These results give clear evidence for the interplay between the mechanisms underlying the stabilization of the ferroelectricity and the modulation of the Mn^{3+} spin structure. However, the main difference here observed relatively to $TbMnO_3$ concerns the effect of the applied magnetic field, having a stronger effect on the modulation wave vector in the Fe-substituted compound in the whole temperature range, while in $TbMnO_3$ the effect is more pronounced in the cycloidal antiferromagnetic phase [12].

In the absence of an applied magnetic field, the (1 0 4) magnetic peak is not observed in the whole temperature range here explored. Under a 1 T strength magnetic field, this reflection appears just below T_N and its intensity increases with decreasing temperature and increasing magnetic field strength, respectively, as can be seen in Fig. 4(a). The appearance of this magnetic peak clearly points out the stabilization of a ferromagnetic component with increasing the magnetic field. Concomitantly, the intensity of the G -type Mn^{3+} moment ordering magnetic superlattice peak ($1 q_{Mn} 3$), shown in Fig. 4(b), only observed below T_C but already at $B = 0$ T, decreases as the magnetic field increases.

The strong changes induced by the applied magnetic field in the neutron diffraction patterns depicted in Fig. 2 point at magnetic phase transformations below the Tb^{3+} ordering temperature. The diffuse scattering signal, observed around the ($0 q_{Mn} 1$) magnetic superlattice peak, which prevails up to

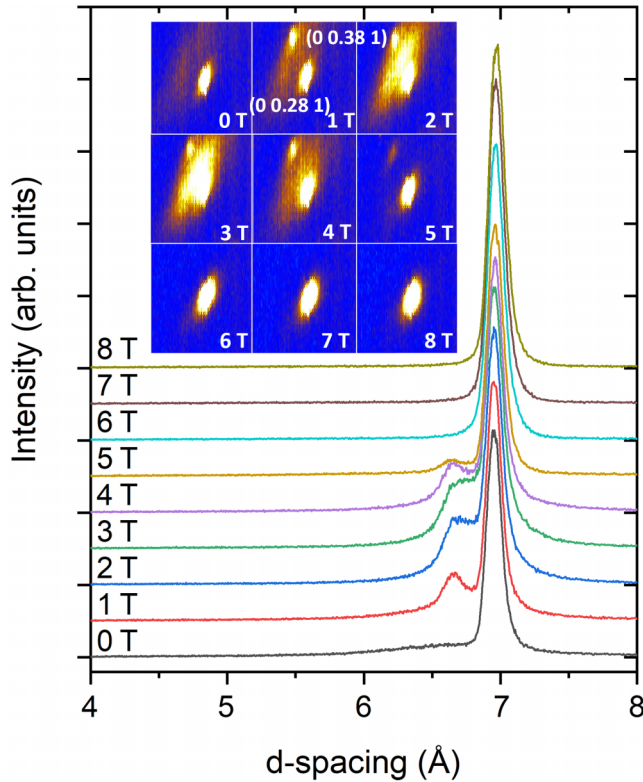


FIG. 5. Neutron diffraction patterns of $\text{TbMn}_{0.98}\text{Fe}_{0.02}\text{O}_3$ recorded at 5 K under several applied magnetic fields along the b axis. The inset shows a detailed view of the neutron diffraction patterns around the $(0\ q_{\text{Mn}}\ 1)$ peak.

4 T, is ascribed to the quite complex and of short-range (local) ordering of Tb^{3+} spins [9,10]. On increasing the magnetic field strength, another magnetic satellite peak starts to be observed, emerging from the diffused scattering signal, as is shown in Fig. 5 for $T = 5$ K. This peak is indexed to the $(0\ 0.38\ 1)$ associated with the modulation of the Tb^{3+} spin structure induced by the applied magnetic field. The intensity and width of this magnetic satellite peak are strongly dependent on the applied magnetic field, and it disappears above 5 T. This result evidences a magnetic field-induced transition of the Tb^{3+} spins, with critical field strength of ~ 5 T, which deserve to be further studied.

IV. DISCUSSION

In this section, we will discuss and correlate the results obtained from polarization and neutron diffraction measurements under magnetic field to unravel the microscopic origin of the magnetically induced ferroelectricity in this compound and its magnetic field dependence. We will address the interplay between magnetism and polar properties, highlighted in Fig. 6, which shows the temperature dependence of the pyroelectric current density and the intensity of the magnetic superlattice peak $(0\ q_{\text{Mn}}\ 1)$, for 0, 4, 6, and 8 T magnetic field strength, applied along the b axis, respectively.

The paramagnetic to incommensurate sinusoidal antiferromagnetic phase transition at T_N is not revealed by any anomaly in the pyroelectric current density, as expected if the

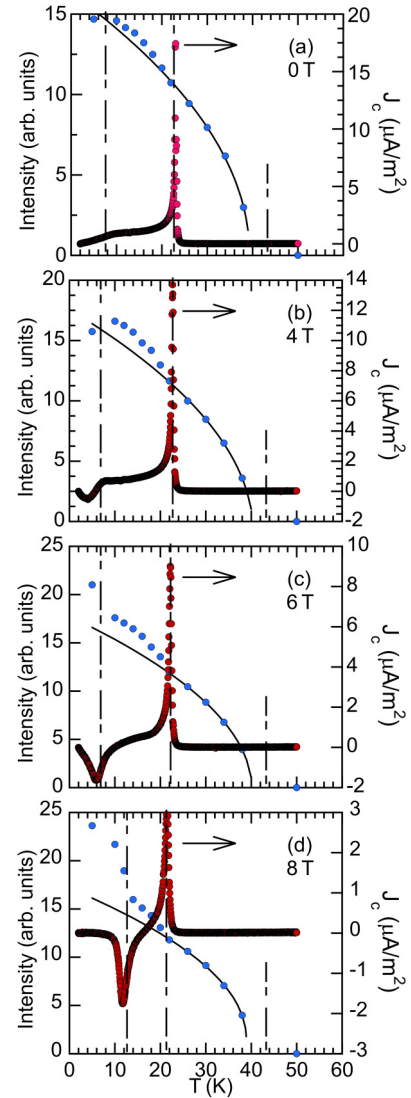


FIG. 6. Temperature dependence of the magnetic superlattice peak $(0\ q_{\text{Mn}}\ 1)$ intensity (left) and the pyroelectric current density (right), measured along the c axis in different magnetic fields applied along the b axis. The solid line represents the temperature trend of the peak intensity in the $T_C < T < T_N$ range, extrapolated to $T < T_C$.

inverse Dzyaloshinskii-Moriya mechanism is assumed only below T_C , like in TbMnO_3 [18,19]. The magnetically induced ferroelectric phase transition is marked by the anomalous temperature dependence of the $(0\ q_{\text{Mn}}\ 1)$ magnetic superlattice peak intensity at T_C . At zero magnetic field, the small anomaly in $J_c(T)$ occurs at 8 K, which is likely associated with the Tb^{3+} spin ordering. The correlation between the anomalous temperature dependence of both $J_c(T)$ and the magnetic superlattice peak $(0\ q_{\text{Mn}}\ 1)$ intensity holds even for applied fields, but following different behavior: at 4 T, $J_c(T)$ exhibits a downward peak at 4 K and the magnetic superlattice peak intensity reaches a maximum value at 10 K; for 6 and 8 T, the downward peak of $J_c(T)$, whose amplitude increases with the field strength, is accompanied by a sudden increase of the slope of the temperature dependence of the magnetic superlattice peak intensity. The spin cycloid is a polar magnetic

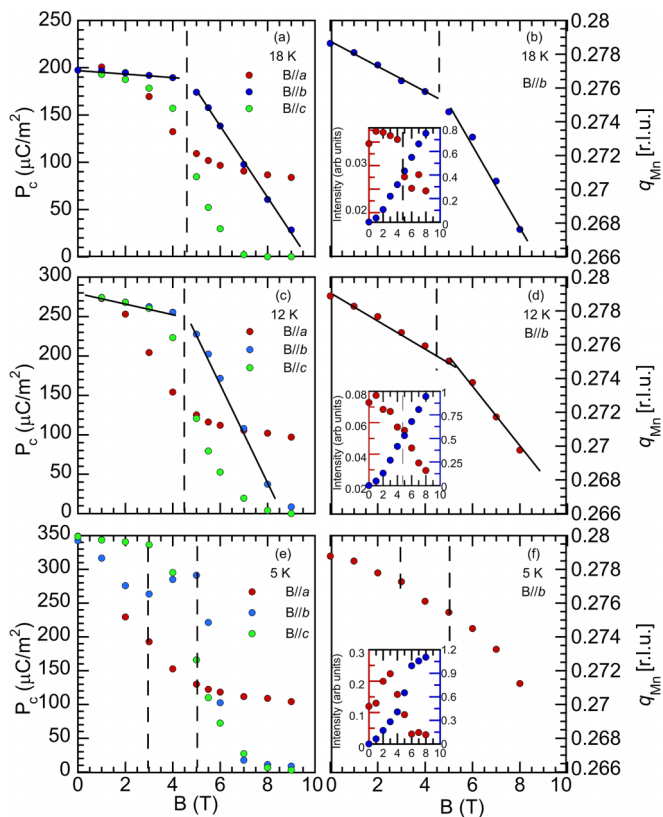


FIG. 7. Magnetic field dependence of the electric polarization P_c measured along the c axis in external magnetic field applied along the $-$, b , and c axes, and the modulation wave vector q_{Mn} , calculated from the $(0 q_{Mn} 1)$ peak position, measured at 18 K (a), (b), 12 K (c), (d), and 5 K (e), (f). Insets: Magnetic field dependence of the intensity of the $(1 q_{Mn} 3)$ magnetic superlattice peak (left red) and the $(1 0 4)$ magnetic peak (right blue).

structure, generating electric polarization in the spin plane, perpendicular to the propagation vector ($\mathbf{P} \sim \mathbf{k} \times (\mathbf{S}_i \times \mathbf{S}_j)$) [18,19]. In the bc -cycloid phase, the electric polarization is expected to be along the c axis, while in the ab -cycloid phase, to be along the a axis. During the cycloid plane rotation from the bc to the ab plane, it is expected an increase of intensity of the $(0 q_{Mn} 1)$ magnetic superlattice peak, simply because in the experimental geometry here described, neutrons probe only the component of magnetic moment perpendicular to the scattering vector, this component being larger when the spins are confined within the ab plane. The results here presented evidence a strong interplay between the modulated magnetic Mn^{3+} spin structure and the stabilization of the electric polarization, as expected in type-II multiferroics.

The interplay between the magnetic structure, electric polarization and magnetoelectric coupling is better ascertained by comparative plots at fixed temperatures. For this purpose, we represent in Fig. 7 the magnetic field dependence of $P_c(T)$, measured with applied magnetic field along the three crystallographic directions, the modulation wave vector q_{Mn} , determined from the magnetic superlattice peak $(0 q_{Mn} 1)$ position, and, in inset, the intensity of the magnetic superlattice $(1 q_{Mn} 3)$ (left axis) and of the ferromagnetic (right axis) peaks. Here we chose to analyze these quantities as a

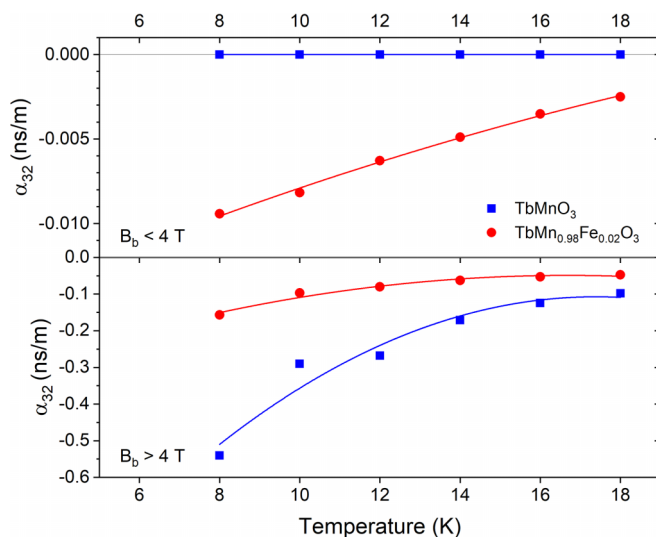


FIG. 8. Temperature dependence of the effective magnetoelectric coefficient α_{32} of TbMnO_3 and $\text{TbMn}_{0.98}\text{Fe}_{0.02}\text{O}_3$ for (a) $B_b < 4 \text{ T}$ and (b) $B_b > 4 \text{ T}$. The solid lines are guide for the eyes. Data concerning TbMnO_3 were taken from Ref. [14].

function of the magnetic field strength at 18 K (for which the a -axis component of the polarization is not observed up to 8 T), 12 K (for which the polarization rotates with applied magnetic field), and 5 K (to study the Tb^{3+} -spin ordering effect), which represent the overall trend of the aforementioned quantities.

For the three chosen representative temperatures, $P_c(B)$ exhibits different magnetic field dependences according to the applied magnetic field direction, mirroring the anisotropic nature of the magnetoelectric coupling. In the 8 to 22 K range, $P_c(B)$ is a linear function of $B \parallel b$ below and above 4.5 T, although with different slopes; it is a linear function of $B \parallel a$ only for $B_a < 4 \text{ T}$ and has a nonlinear dependence with $B \parallel c$, eventually disappearing above a certain value of magnetic field which depends on temperature.

From the slopes of the linear relation between P_c and $B \parallel b$ strength (B_b), we have estimated the effective magnetoelectric coefficient $\alpha_{32} = dP_c/dB_b$ and its temperature dependence is presented in Fig. 8, below and above 4 T.

The effective magnetoelectric coefficient of $\text{TbMn}_{0.98}\text{Fe}_{0.02}\text{O}_3$ is negative, mirroring the decrease the polarization with the magnetic field increase. The value of the magnetoelectric coefficient is one order of magnitude larger for $B_b > 4 \text{ T}$. In both magnetic field ranges, the absolute value α_{32} increases monotonously as temperature decreases, giving evidence for the strengthening of the magnetic field dependence of the electric polarization as the temperature/magnetic field decreases/increases down to 8 K.

Comparing with TbMnO_3 , two different regimes are found, as is clear from Fig. 8. For applied magnetic field strength below 4 T, the effective magnetoelectric coefficient $\alpha_{32} = dP_c/dB_b$ obtained for TbMnO_3 is exactly 0, meaning that while the polarization does not rotate towards the a axis, its value is independent of the applied magnetic field. In contrast, $\text{TbMn}_{0.98}\text{Fe}_{0.02}\text{O}_3$ has a finite negative α_{32} coefficient for the same temperature and magnetic field strength. This result

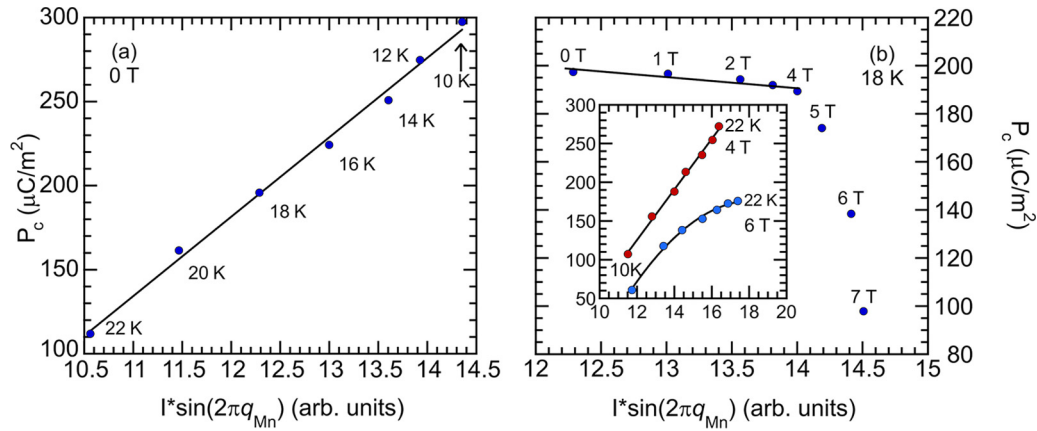


FIG. 9. P_c vs $I \times \sin(2\pi q_{Mn})$ recorded at 0 T for different temperatures (a) and at 18 K with magnetic field $\mathbf{B} \parallel \mathbf{b}$ (b). The intensity I and q_{Mn} values were calculated from the $(0 q_{Mn} 1)$ magnetic superlattice peak. Inset: P_c vs $I \times \sin(2\pi q_{Mn})$ recorded at 4 T and 6 T, for different temperatures.

proves the role played by the Fe^{3+} magnetism, that even a low-level substitution slightly changes the cycloidal ordering, in agreement with the neutron data that show the promotion of a canted structure already at 1 T applied magnetic field. However, above 4 T, the modulus of the effective magnetoelectric coefficient of TbMnO_3 becomes higher than the one calculated for $\text{TbMn}_{0.98}\text{Fe}_{0.02}\text{O}_3$, due to a sharper rotation of the cycloid ordering with the applied magnetic field. The difference between both values increases as temperature decreases, in such a way that at 8 K the effective magnetoelectric coefficient of the pure compound is almost 4 times larger than in the Fe-substituted compound. This demonstrates the strong impact of low-level substitution of Mn^{3+} by Fe^{3+} in the electric polarization dependence on the low applied magnetic field.

Figures 7(b) and 7(d) show the magnetic field dependence of the modulation wave vector q_{Mn} , recorded at 18 K and 12 K, respectively. Two linear regimes in $q_{Mn}(\mathbf{B}_b)$ are ascertained below and above 4.5 T, with a slope increasing from the low to high magnetic field ranges. It is worth stressing that the magnetic field dependence of both $P_c(\mathbf{B}_b)$ and $q_{Mn}(\mathbf{B}_b)$ is rather similar, evidencing a correlation between P_c and the modulated magnetic structure. To discuss the microscopic origin of the magnetically induced ferroelectricity in this compound, we have analyzed the correlation between the electric polarization P_c and the $(0 q_{Mn} 1)$ magnetic superlattice peak characteristics, as it better mirrors the cycloidal spin structure underlying the electric polarization. Following the grounds of the spin current model, presented by Y. Yamasaki *et al.* [20], the electric polarization is predicted to be proportional to the product of $\sin(2\pi q_{Mn})$ and the square of the magnetic structural factor. Unfortunately, the geometric properties of the spin cycloid in this compound could not be determined from our experimental results, and the accurate determination of the magnetic structural factor is not possible. However, we can overcome this difficulty looking at the intensity I of the $(0 q_{Mn} 1)$ magnetic superlattice peak, which is proportional to the square of the magnetic structural factor. Figure 9(a) shows P_c as a function of $I \times \sin(2\pi q_{Mn})$, measured at different temperatures and 0 T. The linear regime observed in the absence of applied field evidences that the mechanism

underlying the magnetoelectric coupling is based on the spin current model applied to a noncolinear spin structure. It is interesting to study the same dependence but at constant temperature and for different applied magnetic field. This study is performed at 18 K where the polarization flip is not observed in the magnetic field range explored in this work. As can be observed in Fig. 9(b), for $B < 4$ T, a linear regime is already found, evidencing that the same microscopic mechanism also prevails in this magnetic field range. However, for $B > 4$ T, a clear deviation of the linear regime is ascertained, enabling us to conclude that the magnetoelectric coupling for $B > 4$ T is not accurately described by the model in Ref. [20]. Actually, the linear dependence of P_c on $I \times \sin(2\pi q_{Mn})$ is broken for magnetic fields above 4 T, as can be observed in the inset of Fig. 9(b). It is worth stressing that q_{Mn} is quite temperature independent for $B < 4$ T, while it becomes strongly temperature dependent for higher fields [see Fig. 3(b)]. The change of magnetic modulation properties at ~ 4 T is undoubtedly in the basis of the change of microscopic mechanisms underlying ferroelectricity. No similar study has been published for TbMnO_3 , to the best of our knowledge, and therefore this work provides a better understanding of the influence of the applied magnetic field on the microscopic mechanisms that induce electric polarization in this class of multiferroics.

Now, we focus on the decrease of P_c of $\text{TbMn}_{0.98}\text{Fe}_{0.02}\text{O}_3$ for $\mathbf{B} \parallel \mathbf{b}$ at 18 K with increasing magnetic field strength. It is worth stressing that at this temperature and for maximum magnetic field strength here applied, no polarization flop occurs. At this temperature, the intensity of the ferromagnetic reflection is a linear increasing function of $\mathbf{B} \parallel \mathbf{b}$, and no anomaly is ascertained at ~ 4.5 T [see inset of Fig. 7(b)], which gives clear evidence for the increase of the ferromagnetic component induced by the applied magnetic field, likely due to a spin canting. The destabilization of the cycloidal Mn^{3+} spin modulation, along with the concomitant appearance of a ferromagnetic component, explain the decrease of the P_c . This result obtained for $\text{TbMn}_{0.98}\text{Fe}_{0.02}\text{O}_3$ contrasts with the one obtained for pure TbMnO_3 from which we conclude that the magnetic field promoted spin canting is a consequence of the Fe spins, even in only 2% concentration [14]. Similar magnetic changes are perceived down to

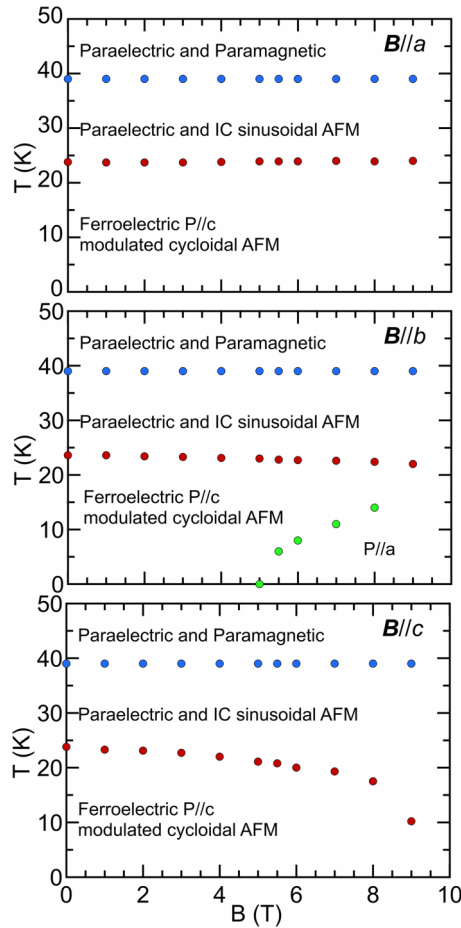


FIG. 10. The magnetolectric phase diagram of $\text{TbMn}_{0.98}\text{Fe}_{0.02}\text{O}_3$, with magnetic fields along the (a) a , (b) b , and (c) c axes. Antiferromagnetic structure has incommensurate sinusoidal modulation between T_N and T_C and cycloidal modulation below T_C .

8 K. Future experiments will be performed to confirm this interpretation.

The magnetolectric coupling at 5 K exhibits different properties. Strictly, q_{Mn} is no longer a linear function of the applied magnetic field [see Fig. 7(f)] and a hint of a downward jump is ascertained at 3.5 T. Interestingly, the magnetic field dependence of the G -type magnetic superlattice peak (1 q_{Mn} 3) intensity exhibits a maximum value at 3 T and becomes magnetic field independent above 5 T, while the (1 0 4) magnetic reflection intensity exhibits an s-shaped anomaly at 5 T. Revisiting Fig. 7(f), we can assign the aforementioned intensity changes at 5 T to the magnetically

induced phase transition. The different behavior described to the one above is a consequence of the Tb^{3+} magnetic ordering on the magnetolectric coupling at 5 K.

To summarize the results here presented, we propose the magnetolectric phase diagram of $\text{TbMn}_{0.98}\text{Fe}_{0.02}\text{O}_3$ shown in Fig. 10, with magnetic fields along the Fig. 10(a) a , Fig. 10(b) b , and Fig. 10(c) c axes.

V. CONCLUSIONS

In this work we report a combined experimental study of the temperature and magnetic field dependence of polarization and magnetic structures in $\text{TbMn}_{0.98}\text{Fe}_{0.02}\text{O}_3$ single crystal. The results show that the low level of Mn^{3+} substitution for Fe^{3+} , although it does not change the phase sequence regarding TbMnO_3 , causes a higher magnetic field sensitivity of the electric polarization for $B < 4$ T. This is due to the changes on the magnetic modulation of the Mn^{3+} spin structure. Two main consequences arise from the magnetic structure changes: (1) the value of the electric polarization is lower than in TbMnO_3 , and (2) the magnetolectric coupling coefficient α_{32} at low magnetic fields below 4 T is finite, ranging between -0.005 ns/m to -0.01 ns/m, contrasting with the vanishing value reported for TbMnO_3 , meaning that while the polarization does not rotate towards the a axis, its value is independent of the applied magnetic field. We attribute this magnetolectric performance enhancement to the effect of the Fe^{3+} magnetism, which alters the magnetic interactions to such an extent that the magnetic structure allowing for ferroelectricity, according to Dzyaloshinskii-Moriya interaction, is no longer stable at high magnetic fields. Our experimental work evidences that the low-level substitution of Mn^{3+} by Fe^{3+} , though keeping the same phase sequence, induces significant changes in properties and evidence for the rather delicate balance between the competitive magnetic interactions underlying the ground state of TbMnO_3 .

ACKNOWLEDGMENTS

This work was supported by the Scientific Grant Agency MŠVVaŠ SR and SAS Project No. VEGA 2/0011/22, the Czech Science Foundation (Project No. 21-06802S), a project from the European Union, and the Czech Ministry of Education, Youth and Sports (Projects No. TERA FIT-CZ.02.01.01/00/22 008/0004594), No. PTDC/FIS-MAC/29454/2017, No. NORTE/01/0145/FEDER/028538, No. IFIM-UP: Norte-070124-FEDER-000070; NECL: NORTE-01-0145-FEDER-022096, No. UIDB/04968/2020, No. UID/NAN/50024/2019, No. PTDC/NAN-MAT/28538/2017, and No. PTDC/FIS/03564/2022.

The authors declare no competing interests.

- [1] S. Dong, J. M. Liu, S. W. Cheong, and Z. Ren, Multiferroic materials and magnetolectric physics: Symmetry, entanglement, excitation, and topology, *Adv. Phys.* **64**, 519 (2015).
- [2] Y. Tokura, S. Seki, and N. Nagaosa, Multiferroics of spin origin, *Rep. Prog. Phys.* **77**, 076501 (2014).
- [3] A. Maia, R. Vilarinho, C. Kadlec, M. Lebeda, M. Mihalik, M. Zentková, M. Mihalik, J. A. Moreira, and S. Kamba, Modifying

the magnetolectric coupling in TbMnO_3 by low-level Fe^{3+} substitution, *Phys. Rev. B* **107**, 104410 (2023).

- [4] M. Mihalik, M. Mihalik, M. Zentková, A. Maia, R. Vilarinho, A. Almeida, J. Agostinho Moreira, J. Pospíšil, and K. Uhlířová, Magnetic properties of $\text{TbMn}_{0.98}\text{Fe}_{0.02}\text{O}_3$ single crystal, *J. Magn. Magn. Mater.* **549**, 168986 (2022).

- [5] M. Mihalik, M. Mihalik, Z. Jagličić, R. Vilarinho, J. A. Moreira, E. Queiros, P. B. Tavares, A. Almeida, and M. Zentková, Magnetic phase diagram of the $\text{TbMn}_{1-x}\text{Fe}_x\text{O}_3$ solid solution system, *Physica B Condens. Matter* **506**, 163 (2017).
- [6] R. Vilarinho, E. Queirós, D. J. Passos, D. A. Mota, P. B. Tavares, M. Mihalik, M. Zentkova, M. Mihalik, A. Almeida, and J. A. Moreira, On the ferroelectric and magnetoelectric mechanisms in low Fe^{3+} doped TbMnO_3 , *J. Magn. Magn. Mater.* **439**, 167 (2017).
- [7] R. Vilarinho, D. J. Passos, E. C. Queirós, P. B. Tavares, A. Almeida, M. C. Weber, M. Guennou, J. Kreisel, and J. A. Moreira, Suppression of the cooperative Jahn-Teller distortion and its effect on the Raman octahedra-rotation modes of $\text{TbMn}_{1-x}\text{Fe}_x\text{O}_3$, *Phys. Rev. B* **97**, 144110 (2018).
- [8] T. Kimura, T. Goto, H. Shintani, K. Ishizaka, T. Arima, and Y. Tokura, Magnetic control of ferroelectric polarization, *Nature (London)* **426**, 55 (2003).
- [9] M. Kenzelmann, A. B. Harris, S. Jonas, C. Broholm, J. Schefer, S. B. Kim, C. L. Zhang, S. W. Cheong, O. P. Vajk, and J. W. Lynn, Magnetic inversion symmetry breaking and ferroelectricity in TbMnO_3 , *Phys. Rev. Lett.* **95**, 087206 (2005).
- [10] R. Kajimoto, H. Yoshizawa, H. Shintani, T. Kimura, and Y. Tokura, Magnetic structure of TbMnO_3 by neutron diffraction, *Phys. Rev. B* **70**, 012401 (2004).
- [11] T. Kimura, S. Ishihara, H. Shintani, T. Arima, K. T. Takahashi, K. Ishizaka, and Y. Tokura, Distorted perovskite with e_g^1 configuration as a frustrated spin system, *Phys. Rev. B* **68**, 060403(R) (2003).
- [12] T. Arima, T. Goto, Y. Yamasaki, S. Miyasaka, K. Ishii, M. Tsubota, T. Inami, Y. Murakami, and Y. Tokura, Magnetic-field-induced transition in the lattice modulation of colossal magnetoelectric GdMnO_3 and TbMnO_3 compounds, *Phys. Rev. B* **72**, 100102(R) (2005).
- [13] T. Goto, T. Kimura, G. Lawes, A. P. Ramirez, and Y. Tokura, Ferroelectricity and giant magnetocapacitance in perovskite rare-earth manganites, *Phys. Rev. Lett.* **92**, 257201 (2004).
- [14] T. Kimura, G. Lawes, T. Goto, Y. Tokura, and A. P. Ramirez, Magnetoelectric phase diagrams of orthorhombic RMnO_3 ($R = \text{Gd, Tb, and Dy}$), *Phys. Rev. B* **71**, 224425 (2005).
- [15] N. Aliouane, D. N. Argyriou, J. Stropfer, I. Zegkinoglou, S. Landsgesell, and M. v. Zimmermann, Field-induced linear magnetoelastic coupling in multiferroic TbMnO_3 , *Phys. Rev. B* **73**, 020102(R) (2006).
- [16] See Supplemental Material at <http://link.aps.org/supplemental/10.1103/PhysRevMaterials.8.084405> for additional information obtained from the neutron diffraction and pyroelectric current experiments and data analysis: diffraction patterns of $\text{TbMn}_{0.98}\text{Fe}_{0.02}\text{O}_3$, recorded at different fixed temperatures and magnetic fields of 2 T and 6 T, applied along the b -axis; the temperature dependence of the a and c lattice parameters of $\text{TbMn}_{0.98}\text{Fe}_{0.02}\text{O}_3$, measured at 0 T and 8 T; and the magnetic field dependence of the electric polarization P_c measured along the c -axis in external magnetic field applied along the a -, b - and c -axes, at fixed temperatures.
- [17] S. Quezel, F. Tcheou, J. Rossat-Mignod, G. Quezel, and E. Roudaut, Magnetic structure of the perovskite-like compound TbMnO_3 , *Physica B+C* **86**, 916 (1977).
- [18] I. A. Sergienko and E. Dagotto, Role of the Dzyaloshinskii-Moriya interaction in multiferroic perovskites, *Phys. Rev. B* **73**, 094434 (2006).
- [19] H. Katsura, N. Nagaosa, and A. V. Balatsky, Spin current and magnetoelectric effect in noncollinear magnets, *Phys. Rev. Lett.* **95**, 057205 (2005).
- [20] Y. Yamasaki, H. Sagayama, T. Goto, M. Matsuura, K. Hirota, T. Arima, and Y. Tokura, Electric control of spin helicity in a magnetic ferroelectric, *Phys. Rev. Lett.* **98**, 147204 (2007).